Ramakrishna Mission Residential College (Autonomous)
Kolkata 700103, WB, India

Collaborative research in coordination chemistry of organic radicals

Number 5

Institute 1: Ramakrishna Mission Residential College (Autonomous)

Concerned Faculty: Dr. Prasanta Ghosh, Dept of Chemistry

&

Institute 2: Max-Planck-Institut für Chemische Energiekonversion

Stiftstrasse 34 - 36 / D - 45470 Mülheim an der Ruhr

Concerned Scientist: Dr Thomas Weyhermüller

Period of Investigation: 30-10-2015 to 28-03-2016

Project: Radical states of the [Ru(PIQ)] core in complexes (PIQ = 9,10-phenanthreneiminoquinone)

Output: The result was published in a journal of international repute

Publication: Radical non-radical states of the [Ru(PIQ)] core in complexes (PIQ = 9,10-phenanthreneiminoquinone)

Sachinath Bera, Suvendu Maity, Thomas Weyhermüller and Prasanta Ghosh*

Dalton Trans., 2016, *45*, 8236-8247

Dr. Prasanta Ghosh

Dr Thomas Weyhermüller

Dalton Transactions

PAPER

Radical non-radical states of the [Ru(PIQ)] core in complexes (PIQ = 9,10-phenanthreneiminoquinone)†

Sachinath Bera,[a] Suvendu Maity,[a] Thomas Weyhermüller[b] and Prasanta Ghosh*[a]

Cite this: *Dalton Trans.*, 2016, **45**, 8236

9,10-Phenanthreneiminosemiquinonate anion radical ($PIQ^{\bullet-}$) complexes of ruthenium of types *trans*-$[Ru^{II}(PIQ^{\bullet-})(PPh_3)_2(CO)Cl]$ (**1**) and *trans*-$[Ru^{III}(PIQ^{\bullet-})(PPh_3)_2Cl_2]$ (**2**) are reported. Reactions of **1** and **2** with I_2 afford *trans*-$[Ru^{III}(PIQ^{\bullet-})(PPh_3)_2(CO)Cl]^+I_3^-\cdot\frac{1}{2}CH_2Cl_2$ ($\mathbf{1}^+I_3^-\cdot\frac{1}{2}CH_2Cl_2$) and *trans*-$[Ru_2^{III}(PIQ^{\bullet-})_2(PPh_3)_2(\mu\text{-}Cl)_3]^+I_3^-\cdot\frac{1}{4}I_2\cdot\frac{1}{4}$toluene) ($\mathbf{3}^+I_3^-\cdot\frac{1}{4}I_2\cdot\frac{1}{4}$toluene), while the reaction of **2** with Br_2 yields a 9,10-phenanthreneiminoquinone (PIQ) complex of the type *mer*-$[Ru^{III}(PIQ)(PPh_3)Br_3]\cdot\frac{1}{2}CH_2Cl_2$ ($\mathbf{4}\cdot\frac{1}{2}CH_2Cl_2$). In comparison, the reaction of *trans*-$[Ru^{III}(PQ^{\bullet-})(PPh_3)_2Cl_2]$ ($\mathbf{2}_{PQ}$), a 9,10-phenanthrenequinone (PQ) analogue of **2** affords only *trans*-$[Ru^{III}(PQ)(PPh_3)_2Cl_2]^+Br_3^-$ ($\mathbf{5}^+Br_3^-$). Considering the X-ray bond parameters, EPR spectra and the atomic spin densities obtained from the density functional theory (DFT) calculations, **1** is defined as a $PIQ^{\bullet-}$ (average C–O/N and C–C lengths, 1.280(2) and 1.453(3) Å) complex of ruthenium(II) while **4** is a neutral PIQ (average C–O, C–N, C–C and C–O/N lengths, 1.248(7), 1.284(7), 1.485(8) and 1.266(7) Å) complex of the ruthenium(III) ion. The single crystal X-ray bond parameters proposed that $\mathbf{1}^+I_3^-$ (average C–O/N and C–C lengths, 1.294(8) and 1.449(9) Å) and **2** (average C–O/N and C–C lengths, 1.289(2) and 1.447(4) Å) are $PIQ^{\bullet-}$ complexes of ruthenium(III), while the $\mathbf{3}^+$ ion (average C–O/N and C–C lengths, 1.288 ± 0.004 and 1.450 ± 0.017 Å) is a co-facial bi-octahedral complex of ruthenium(III). In contrast, the $\mathbf{5}^+$ ion is a PQ complex of the ruthenium(III) ion. EPR spectra and the calculated atomic spin densities authenticated that the $\mathbf{2}^+$ ion obtained after constant potential coulometric oxidation of **2** is a PIQ complex of ruthenium(III), while the $\mathbf{2}^-$ ion is a hybrid state of $[Ru^{II}(PIQ^{\bullet-})]$ and $[Ru^{III}(PIQ^{2-})]$ states. It is observed that the $PIQ^{\bullet-}$ state in which spin is more localized on the nitrogen (~38% in **1** and ~35% in $\mathbf{2}^-$ ion) is stable and the coordination of the PIQ^{2-} state is not observed in this study. Redox activities, UV-vis/NIR absorption spectra and their origins and the spectroelectrochemical measurements for $\mathbf{2} \rightarrow \mathbf{2}^+$, $\mathbf{2} \rightarrow \mathbf{2}^-$ and $\mathbf{3}^+ \rightarrow \mathbf{3}^{2+}$ conversions are analyzed.

Received 8th January 2016,
Accepted 5th April 2016

DOI: 10.1039/c6dt00091f

www.rsc.org/dalton

Introduction

Redox active or redox non-innocent ligands are capable of expanding the redox activity of the coordinated metal ion and promoting metal ions to take part in catalysis.[1] These ligands participate in the electron transfer reaction relatively at a lower potential and the electronic structures of the complexes particularly containing redox active transition metal ions are complex.[2] In this context, the redox chemistry of *o*-amino phenols is encouraging and expanding fast.[3] However, the related chemistry of 9,10-phenanthreneiminoquinone (PIQ), an analogue of *o*-iminobenzoquinone did not grow; only one complex has been reported so far.[4] In this article the versatile redox chemistry of PIQ in ruthenium complexes incorporating PPh_3, CO and halide as co-ligands is reported.

In complexes PIQ can exist as PIQ, a 9,10-phenanthreneimino semiquinonate anion radical ($PIQ^{\bullet-}$) and 10-amidophenanthren-9-olato (PIQ^{2-}) as illustrated in Scheme 1. In this study, the controlled reduction of PIQ by a hydridoruthenium

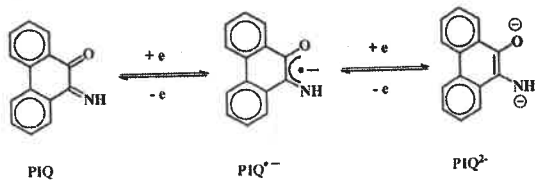

Scheme 1 Redox activity of PIQ.

[a]*Department of Chemistry, R. K. Mission Residential College, Narendrapur, Kolkata-103, India. E-mail: ghosp@pghosh.in*

[b]*Max-Planck-Institut für Chemische Energiekonversion, Stiftstrasse 34-36, D-45470 Mülheim, Germany*

†Electronic supplementary information (ESI) available: X-ray crystallographic CIF files for **1**, $\mathbf{1}^+I_3^-\cdot\frac{1}{2}CH_2Cl_2$, **2**, $\mathbf{3}^+I_3^-\cdot\frac{1}{4}I_2\cdot\frac{1}{4}$toluene, $\mathbf{4}\cdot\frac{1}{2}CH_2Cl_2$ and $\mathbf{5}^+Br_3^-$; EPR data; cyclic voltammograms; gas phase optimized coordinates of $\mathbf{1}^{Me}$, $\mathbf{1}^{Me+}$, $\mathbf{2}^{Me}$, $\mathbf{2}^{Me+}$, $\mathbf{2}^{Me-}$ and $\mathbf{4}^{Me}$ excitation energies, oscillator strengths, transition types and dominant contributions of UV-vis/NIR absorption bands from TD DFT calculations. CCDC 1442782–1442786 and 1454005. For ESI and crystallographic data in CIF or other electronic format see DOI: 10.1039/c6dt00091f

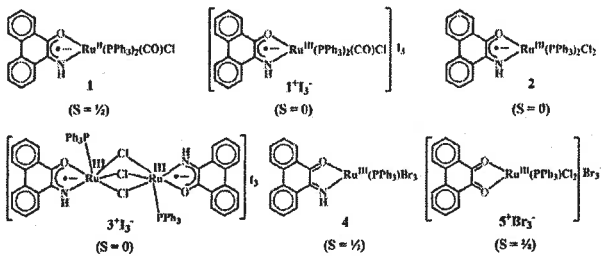

Chart 1 Isolated complexes of $PIQ^{\bullet-}$, PIQ and PQ with ruthenium(II/III) ions.

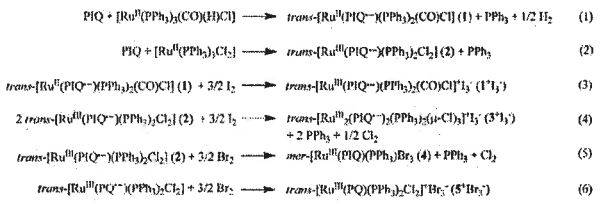

Chart 2 Synthetic reactions of the complexes.

(II) precursor affording a $PIQ^{\bullet-}$ complex was authenticated. The PIQ and $PIQ^{\bullet-}$ complexes reported in this article are summarized in Chart 1. The $PIQ^{\bullet-}$ complexes of types *trans*-$[Ru^{II}(PIQ^{\bullet-})(PPh_3)_2(CO)Cl]$ (**1**) and *trans*-$[Ru^{III}(PIQ^{\bullet-})(PPh_3)_2Cl_2]$ (**2**) were isolated and their reactions with halogens were investigated. The related chemistry is compared with that of *o*-aminophenol and PQ ligands.[5] The reaction of **1** with I_2 solution afforded *trans*-$[Ru^{III}(PIQ^{\bullet-})(PPh_3)_2(CO)Cl]^+I_3^-\cdot\frac{1}{2}CH_2Cl_2$ ($\mathbf{1}^+I_3^-\cdot\frac{1}{2}CH_2Cl_2$), while the reaction of **2** with I_2 solution yielded *trans*-$[Ru^{III}_2(PIQ^{\bullet-})_2(PPh_3)_2(\mu\text{-}Cl)_3]^+I_3^-\cdot\frac{1}{4}I_2\cdot\frac{1}{4}$toluene ($\mathbf{3}^+I_3^-\cdot\frac{1}{4}I_2\cdot\frac{1}{4}$toluene) as an isolable product. The 3^+ ion is a co-facial bi-octahedral complex of ruthenium(III) incorporating a redox non-innocent ligand. Bi-octahedral complexes of the $[Ru(\mu\text{-}Cl)_3Ru]$ core incorporating redox non-innocent ligands are rare. In this regard, the isolation of $\mathbf{3}^+I_3^-\cdot\frac{1}{4}I_2\cdot\frac{1}{4}$toluene is worthy. The reaction of **2** with Br_2 solution does not promote dimerization, rather it generated a ruthenium(III) complex of PIQ of the type *mer*-$[Ru^{III}(PIQ)(PPh_3)Br_3]\cdot\frac{1}{2}CH_2Cl_2$ ($\mathbf{4}\cdot\frac{1}{2}CH_2Cl_2$). In contrast, the reaction of *trans*-$[Ru^{III}(PQ^{\bullet-})(PPh_3)_2Cl_2]$ ($\mathbf{2}_{PQ}$),[5] a 9,10-phenanthreneimino quinone (PQ) analogue of **2**, with Br_2 neither afforded PQ analogues of 3^+ nor **4** but yielded a PQ complex of ruthenium(III) of the type *trans*-$[Ru^{III}(PQ)(PPh_3)_2Cl_2]^+Br_3^-$ ($\mathbf{5}^+Br_3^-$). **1**, $\mathbf{1}^+I_3^-\cdot\frac{1}{2}CH_2Cl_2$, **2**, $\mathbf{3}^+I_3^-\cdot\frac{1}{4}I_2\cdot\frac{1}{4}$toluene, $\mathbf{4}\cdot\frac{1}{2}CH_2Cl_2$ and $\mathbf{5}^+Br_3^-$ were substantiated by different spectra, single crystal X-ray structure determinations and density functional theory (DFT) calculations.

Results and discussion

Syntheses and characterization

PIQ was prepared by a reported procedure.[6] The complexes were generated following the reactions as depicted in Chart 2. **1** was isolated in good yields from a reaction of PIQ with $[Ru^{II}(PPh_3)_3(CO)(H)Cl]$[7] in boiling toluene. It is an example of the controlled reduction of PIQ by one electron using the Ru^{II}–H precursor as given by eqn (1). Similar reactions were substantiated using PQ and azo-pyridine as ligands.[5a,b,d] The reaction of PIQ with $[Ru^{II}(PPh_3)_3Cl_2]$[7] afforded **2**. The oxidation of **1** in CH_2Cl_2 with I_2 in *n*-hexane gave $\mathbf{1}^+I_3^-\cdot\frac{1}{2}CH_2Cl_2$. The coulometric oxidation of **2** at a constant potential generated $\mathbf{2}^+$, while the oxidation of **2** by I_2 solution in a dichloromethane/toluene mixture produced a diamagnetic co-facial bi-octahedral ruthenium(III) complex, $\mathbf{3}^+I_3^-\cdot\frac{1}{4}I_2\cdot\frac{1}{4}$toluene in lower yields.

The reaction of **2** with Br_2 solution afforded a mononuclear ruthenium(III) bromo complex, $\mathbf{4}\cdot\frac{1}{2}CH_2Cl_2$, while a similar reaction with $\mathbf{2}_{PQ}$ produced the 5^+ ion.

Details of the syntheses of the complexes are outlined in the Experimental section. *Trans* abbreviation of the complexes is due to the two PPh_3 ligands which lie *trans* to each other. The complexes were characterized by elemental analyses, mass spectra, IR and ^1H NMR spectra. The data are listed in the Experimental section. The N–H stretching vibrations of the complexes are observed in the range of 3380–3440 cm^{-1}. The $\nu_{C=O}$ and $\nu_{C=N}$ of **4** are relatively higher (1635 and 1621 cm^{-1}) than those (1481–1434 cm^{-1}) of **1**, $\mathbf{1}^+I_3^-$, **2** and $\mathbf{3}^+I_3$. The $\nu_{C=O}$ of **1** appears at 1928 cm^{-1} while the same in $\mathbf{1}^+I_3^-$ is observed at 2017 cm^{-1} indicating the oxidation of ruthenium(II) to ruthenium(III) in $\mathbf{1}^+I_3^-$. It is noteworthy that the conversion of *trans*-$[Ru^{II}(PQ^{\bullet-})(PPh_3)_2(CO)Cl]$[5] to *trans*-$[Ru^{II}(PQ)(PPh_3)_2(CO)Cl]^+I_3^-$ blue shifts the $\nu_{C=O}$ only by 30 cm^{-1}.

The monocationic di-nuclear complex can be presented by the three valence tautomers varying the charge of the PIQ ligands *vis-à-vis* the oxidation state of the ruthenium ions as illustrated in Chart 3. The X-ray bond parameters of the PIQ chelate were used to differentiate between the Ru(III, III) and Ru(II, II) states. Considering the single crystal X-ray bond parameters of $\mathbf{3}^+I_3^-\cdot\frac{1}{4}I_2\cdot\frac{1}{4}$toluene (*vide infra*), the molecule is defined approximately as a $PIQ^{\bullet-}$ complex of the Ru(III, III) state as depicted in Chart 3. In the UV-vis/NIR spectrum, the 3^+ ion does not exhibit any intervalence charge transfer band[8] (*vide*

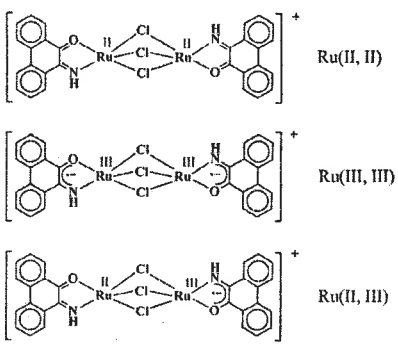

Chart 3 Valence tautomers of the 3^+ (PPh_3 is omitted for clarity) ion defining the states by the oxidation state of the ruthenium ion.

infra) and excludes the possibility of the existence of the mixed valence Ru(II, III) state.

Assignment of the electronic states of the complexes

The electronic structures of the complexes were elucidated by the X-ray bond parameters, EPR spectra and atomic spin population analyses. The single crystal X-ray structures of the complexes were determined at 100 or 295 K. The crystallographic data are summarized in Table S1.† The redox state of the PIQ ligand in complexes was elucidated using the X-ray bond parameters. For comparison, we have considered two paramagnetic molecules as standards: $1{\cdot}CH_2Cl_2$ for $PIQ^{\bullet-}$ and $4{\cdot}\frac{1}{2}CH_2Cl_2$ for PIQ states. The EPR measurement parameters are summarized in Table S2.† The DFT calculations were performed on the model complexes containing PMe_3 instead of PPh_3 ligands. The gas phase geometry of *trans*-$[Ru^{III}(PIQ^{\bullet-})(PMe_3)_2Cl_2]$ (2^{Me}) was optimized with the singlet and triplet spin states while, *trans*-$[Ru^{II}(PIQ)(PMe_3)_2(CO)Cl]^+$ (1^{Me+}) was optimized with singlet spin state only. The geometries of *trans*-$[Ru^{II}(PIQ^{\bullet-})(PMe_3)_2(CO)Cl]$ (1^{Me}), *trans*-$[Ru^{II}(PIQ)(PMe_3)_2(CO)Cl]^+$ (1^{Me+}), *trans*-$[Ru^{III}(PIQ)(PMe_3)_2Cl_2]^+$ (2^{Me+}), *trans*-$[Ru^{II}(PIQ^{\bullet-})(PMe_3)_2Cl_2]^-$ (2^{Me-}) and *mer*-$[Ru^{III}(PIQ)(PMe_3)Br_3]$ (4^{Me}) were optimized with the doublet spin state and the optimized coordinates are listed in Tables S3–S10.†

$1{\cdot}CH_2Cl_2$ crystallizes in the *C2/c* space group. The molecular geometry with the atomic labelling scheme is depicted in Fig. 1(a). The bond parameters are summarized in Table 1. The (CO, Cl) and (O, NH) pairs are disordered along a C_2 axis which bisects the C2–C2A and C8–C8A bonds of the PIQ fragment. The average Ru^{II}–O/N and Ru^{II}–PPh_3 lengths are 2.017 (2) and 2.393(1) Å. The Ru^{II}–Cl distance is 2.446(2) Å. The relatively longer average C–O/N lengths, 1.280(2) Å, and the relatively shorter C–C length, 1.453(3) Å, of the PIQ chelate in comparison with those reported in *o*-iminobenzoquinone[9] infer the existence of the $[Ru^{II}(PIQ^{\bullet-})]$ state in **1**. The X-ray

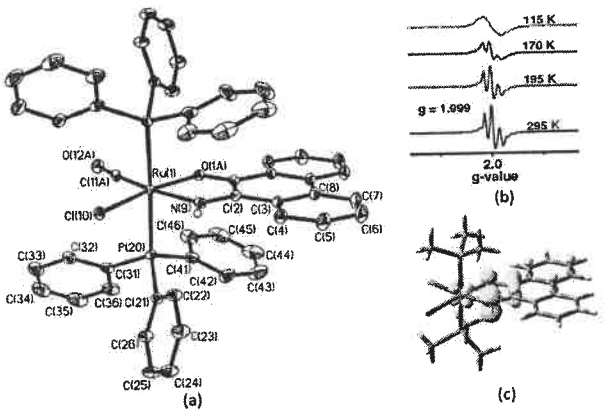

Fig. 1 (a) Molecular geometry of $1{\cdot}CH_2Cl_2$ in crystals (40% thermal ellipsoids; CH_2Cl_2 and H atoms are omitted for clarity), (b) variable temperature (295–115 K) X-band EPR spectra of **1** in CH_2Cl_2 and (c) atomic spin density plot of 1^{Me} obtained from Mulliken spin population analysis (Ru1, 0.09; O1A, 0.16; N9, 0.38; C2A, 0.19; C2, 0.04).

Table 1 Selected experimental bond lengths (Å) of $1{\cdot}CH_2Cl_2$ and $4{\cdot}\frac{1}{2}CH_2Cl_2$ and the corresponding calculated parameters of 1^{Me} and 4^{Me} obtained from B3LYP/DFT calculations

Bonds	Exptl $1{\cdot}CH_2Cl_2$	Calcd 1^{Me}	Exptl[a] $4{\cdot}\frac{1}{2}CH_2Cl_2$	Calcd 4^{Me}
Ru–O	2.071(2)	2.176	2.121(4)/2.121(4)	2.163
Ru–N	2.071(2)	2.060	2.060(5)/2.060(5)	2.076
Ru–PPh_3	2.393(1)	2.419/2.418	2.329(3)/2.309(3)	2.352
Ru–X	2.446(2)	2.494	2.473(3)/2.466(3)	2.541
Ru–CO	1.835(4)	1.852		
C–O	1.280(2)	1.297	1.249(7)/1.247(7)	1.248
C–N		1.344	1.265(7)/1.303(7)	1.299
C–C	1.453(3)	1.429	1.490(8)/1.481(8)	1.484

[a] Unit cell contains two independent molecules.

bond parameters of **1** correlate well with those of the $[Ru^{II}(PQ^{\bullet-})]$ state reported recently.[5]

The X-band EPR spectrum of the powder of **1** at 295 K as illustrated in Fig. S1(a)† corresponding to $g = 1.997$ is consistent with the existence of $PIQ^{\bullet-}$ coordinated to the ruthenium(II) ion. The variable temperature EPR spectra of **1** in CH_2Cl_2 are depicted in Fig. 1(b). The isotropic EPR signal of **1** in CH_2Cl_2 at 295 K at $g = 1.999$ was simulated considering the hyperfine couplings due to ^{14}N ($I = 1$, $A_N = 10.81$), ^{31}P ($I = \frac{1}{2}$, $A_P = 25.38$ G) and ^1H ($I = \frac{1}{2}$, $A_H = 11.20$ G) nuclei as shown in Fig. S1(b).† The frozen CH_2Cl_2 glass EPR spectrum of **1** at 115 K is relatively broader and the hyperfine splitting is not observed.

The density functional theory (DFT) calculation on 1^{Me} further supports the existence of the $PIQ^{\bullet-}$ state in **1**. The gas phase geometry of 1^{Me} with the doublet spin state was optimized at the B3LYP level of theory and the significant optimized bond parameters are listed in Table 1. The calculated lengths are approximately similar to those of $1{\cdot}CH_2Cl_2$. The calculated average C–O/N, 1.320 Å and C–C, 1.429 Å lengths of the chelate correlate well with those of *o*-iminobenzosemiquinonate anion radicals.[10] The atomic spin density as shown in Fig. 1(c), obtained from Mulliken spin population analysis is dominantly dispersed on the PIQ backbone, significantly, ~38% spin being localized on a nitrogen p-orbital. It authenticates the reduction of PIQ to $PIQ^{\bullet-}$, inferring a major contribution of the $Ru^{II}(PIQ^{\bullet-})$ state to the ground electronic state of **1**. However, the localization of 9.3% spin on one of the t_{2g} orbitals of the ruthenium ion predicts a minor contribution of the $[Ru^{III}(PIQ^{2-})]$ state to the electronic state of **1** as predicted from the frozen CH_2Cl_2 glass EPR spectrum of **1**. The calculated coupling constants due to ^{14}N, ^{31}P and ^1H nuclei respectively 8.73, 19.3 and 9.5 G are similar to those obtained experimentally from the fluid solution EPR spectrum of **1**.

$4{\cdot}\frac{1}{2}CH_2Cl_2$ crystallizes in the $P2_1/c$ space group. The molecular geometry with the atomic labelling scheme is shown in Fig. 2(a). The significant bond parameters are summarized in Table 1. The average Ru^{III}–Br and Ru^{III}–PPh_3 lengths are 2.469 (7) and 2.318(2) Å. The average Ru–O and Ru–N lengths are 2.121(4) and 2.060(5) Å. The average C–O and C–N lengths, 1.248(7) and 1.284(7) Å, are shorter than those in $1{\cdot}CH_2Cl_2$. The relatively shorter average C–O/N lengths, 1.266(7) Å and

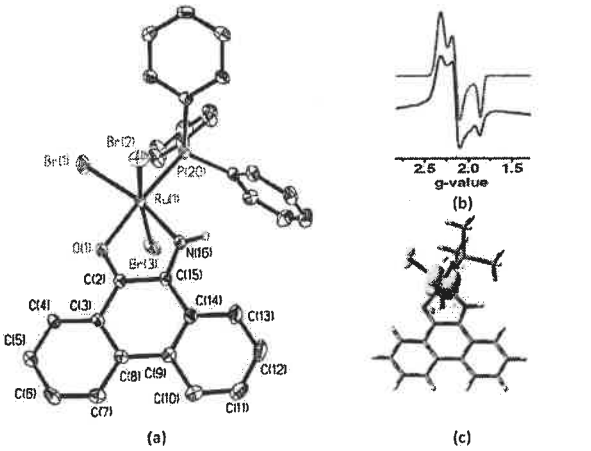

Fig. 2 (a) Molecular geometry of $4{\cdot}\frac{1}{2}CH_2Cl_2$ in crystals (40% thermal ellipsoids; H atoms and CH_2Cl_2 are omitted for clarity); (b) X-band EPR spectra of 4 at 115 K in CH_2Cl_2 (black, exp; red, simulated); (c) atomic spin density plots of 4^{Me} obtained from Mulliken spin population analyses (Ru1, 0.87).

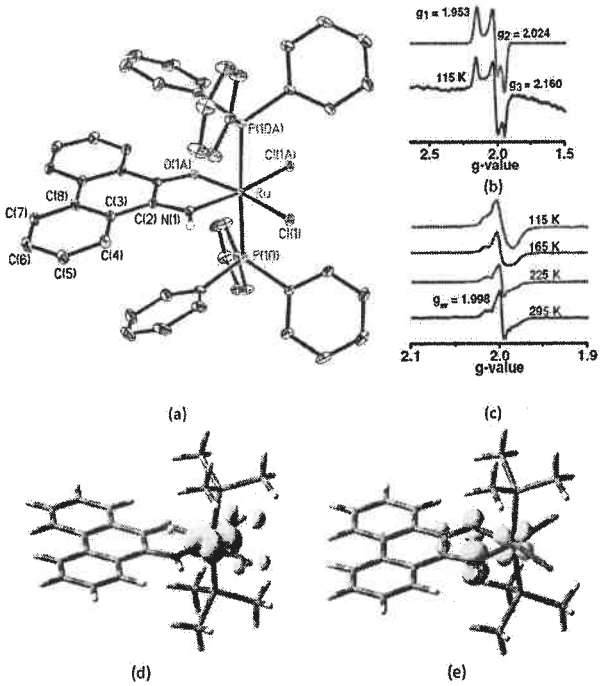

Fig. 3 (a) Molecular geometry of 2 in crystals (40% thermal ellipsoids; H atoms are omitted for clarity); X-band EPR spectra of (b) 2^+ at 115 K (black, experimental; red, simulated) and (c) 2^- at 295–115 K in CH_2Cl_2; atomic spin density plots of (d) 2^{Me+} (Ru, 0.90) and (e) 2^{Me-} (Ru, 0.32; O1, 0.13; N1, 0.35; C2, 0.12) obtained from Mulliken spin population analyses.

the longer C–C length, 1.485(8) Å of the chelate corroborate well with those reported for *o*-iminobenzoquinone complexes,[9] inferring the existence of neutral PIQ in $4{\cdot}\frac{1}{2}CH_2Cl_2$. It is the first example of a PIQ complex of a transition metal ion. The PQ analogue of 4 is not known in the literature.

The CH_2Cl_2 frozen glass EPR spectrum of 4 at 115 K was recorded and is illustrated in Fig. 2(b). The anisotropic EPR spectrum with $g_1 = 2.323$, $g_2 = 2.154$ and $g_3 = 1.881$ is consistent with the existence of the $[Ru^{III}(PIQ)]$ state in $4{\cdot}\frac{1}{2}CH_2Cl_2$. The calculated bond parameters of 4^{Me} as listed in Table 1 correlate well with those obtained from the single crystal X-ray structure of $4{\cdot}\frac{1}{2}CH_2Cl_2$. The average C–O/N lengths are relatively shorter than those of 1^{Me}. The atomic spin density as illustrated in Fig. 2(c) is dominantly localized on the ruthenium ion corroborating with the ruthenium(III) state of 4, as predicted from the X-ray bond parameters and the frozen glass EPR spectrum.

2 crystallizes in the *C*2/*c* space group. The molecular geometry with the atomic labelling scheme is illustrated in Fig. 3(a). The bond parameters are summarized in Table 2. Similar to $1{\cdot}CH_2Cl_2$, 2 contains a C_2 axis that bisects the PIQ ligand and results in disordered O/NH sites. The average Ru–O/N, 1.995(2) and Ru–Cl, 2.388(1) Å lengths are relatively shorter than those of $1{\cdot}CH_2Cl_2$, while the average Ru–PPh_3 (π-acidic ligand) lengths, 2.409(1) Å, are relatively longer. The trend is consistent with the oxidation of ruthenium(II) to ruthenium(III) in 2.

The average C–O/N, 1.289(2) Å lengths are relatively longer than those of $4{\cdot}CH_2Cl_2$, while the C–C, 1.447(4) Å length is relatively shorter. These bond parameters of the chelate are closer to those of the $PIQ^{\bullet-}$ state as observed in the case of 1. Thus, $[Ru^{III}(PIQ^{\bullet-})]$ is considered to be a major component of the ground electronic state of 2. The chemistry parallels to that of PQ have been documented recently. With *o*-aminophenols, a similar $[Ru^{III}(ISQ^{\bullet-})]$ ($ISQ^{\bullet-}$ = *o*-iminobenzosemiquinonate anion radical) state was substantiated.[5]

The frozen CH_2Cl_2 glass EPR spectrum of the 2^+ ion recorded at 115 K is illustrated in Fig. 3(b). The anisotropic spectrum with $g_1 = 1.953$, $g_2 = 2.024$, and $g_3 = 2.160$ is consistent with the ruthenium(III) state of the 2^+ ion. The CH_2Cl_2 solution and frozen glass EPR spectra of the 2^- ion are illustrated in Fig. 3(c). The EPR signal at $g = 1.998$ in CH_2Cl_2 at 295 K is consistent with the $[Ru^{II}(PIQ^{\bullet-})]$ description of the 2^- ion. No anisotropic spectrum due to the ruthenium(III) state was resolved even in frozen glass at 115 K. However, in the case of the PQ analogue the contribution of the $[Ru^{III}(PQ^{2-})]$ state is observable.[5]

The calculated bond parameters of 2^{Me} are similar to those obtained from the single crystal X-ray diffraction study of 2. The average C–O/N (1.309 Å) and the C–C lengths (1.437 Å) of the chelate of 2^{Me} correlate well with those of 1^{Me}. However, at the B3LYP level of theory the closed shell singlet (CSS) solution of 2^{Me} is stable, may be due to a significant contribution of the $[Ru^{II}(PIQ)]$ state to 2. Notably, the calculated energies of the CSS and the open shell singlet (OSS) solutions of 2^{Me} are the same, however the energy of the triplet solution is 21.2 kJ mol^{-1} higher than the singlet solutions.

The calculated average C–O/N and C–C lengths of the chelate of the 2^{Me+} ion are 1.289 and 1.469 Å predicting a

Table 2 Selected experimental bond lengths (Å) of $1^{+}I_3^{-}\cdot\frac{1}{2}CH_2Cl_2$ and **2** and corresponding calculated parameters 1^{Me+}, 2^{Me}, 2^{Me+} and 2^{Me-} obtained from B3LYP/DFT calculations

	Exptl	Calcd	Exptl	Calcd		
Bonds	$1^{+}I_3^{-}\cdot\frac{1}{2}CH_2Cl_2$	1^{Me+}	**2**	2^{Me}	2^{Me+}	2^{Me-}
Ru–O	2.141(4)	2.189	1.995(2)	2.127	2.106	2.139
Ru–N	1.993(5)	2.024	1.995(2)	1.936	2.034	1.994
Ru–PPh_3	2.411(2)	2.450	2.409(1)	2.416	2.459	2.387
	2.424(2)	2.453		2.414	2.457	2.386
Ru–Cl	2.440(3)	2.450	2.388(1)	2.506/2.467	2.356/2.369	2.522/2.556
Ru–CO	1.852(8)	1.859				
C–O	1.268(7)	1.262	1.289(2)	1.279	1.267	1.302
C–N	1.320(8)	1.316		1.339	1.311	1.355
C–O/N (avg)	1.294(8)	1.289	1.289(2)	1.309	1.289	1.328
C–C (chelate)	1.449(9)	1.472	1.447(4)	1.437	1.469	1.423

major contribution of the $[Ru^{III}(PIQ)]$ state to the 2^{Me+} ion. In the 2^{Me+} ion the atomic spin is primarily localized to the ruthenium ion (d_{xy} orbital) as depicted in Fig. 3(d). In contrast, the atomic spin of the 2^{Me-} ion scatters on both ruthenium ion (d_{yz} orbital) and PIQ backbone as shown Fig. 3(e), attributed to contributions of the $[Ru^{III}(PIQ^{2-})]$ and $[Ru^{II}(PIQ^{\bullet-})]$ states to the 2^{-} ion, which makes the frozen glass EPR spectrum relatively broader. The atomic spin is significantly (~35%) localized on one of the p-orbitals of the nitrogen atom. The calculated average C–O/N length of 2^{Me-} is expectedly longer, 1.328 Å, while the C–C length is relatively shorter, 1.423 Å and compares well with those of 1^{Me} and 2^{Me}.

$1^{+}I_3^{-}\cdot\frac{1}{2}CH_2Cl_2$ crystallizes in the *C*2/*c* space group. The molecular geometry with the atomic labelling scheme is illustrated in Fig. 4(a). The average Ru–O/N and Ru–PPh_3 lengths are similar to those of $1\cdot CH_2Cl_2$. However, the C–O and C–N lengths, 1.268(7) and 1.320(8) Å, the average C–O/N being 1.294(8) Å, are relatively longer than those of $4\cdot\frac{1}{2}CH_2Cl_2$. The C–C, 1.449(2) Å length, similar to those of the $PIQ^{\bullet-}$ state in $1\cdot CH_2Cl_2$ and **2**, is relatively shorter. Thus, a major contribution of the $[Ru^{III}(PIQ^{\bullet-})]$ state to $1^{+}I_3^{-}\cdot\frac{1}{2}CH_2Cl_2$ is predicted. It is a rare example of a cationic complex that contains a reduced anion radical.[2e,g] It is noteworthy that *trans*-$[Ru^{II}(PQ)(PPh_3)_2(CO)Cl]^{+}$ is a PQ complex of ruthenium(II).[5]

The calculated bond parameters of the gas phase geometry of 1^{Me+} as listed in Table 2 are notable. The average C–O/N lengths are 1.289 Å which are shorter than those obtained in the case of 1^{Me}. It is due to the contribution of the $[Ru^{II}(PIQ)]$ state to the 1^{Me+} ion.

$3^{+}I_3^{-}\cdot\frac{1}{4}I_2\cdot\frac{1}{4}$toluene crystallizes in the $P2_1$ space group. The molecular geometry with the atomic labelling scheme is illustrated in Fig. 4(b). In the unit cell four independent bi-octahedral 3^{+} ions are present and their significant bond parameters are listed in Table 3. The average Ru–Ru distances are 3.166(12) Å, which are relatively longer than that of the $[Ru_2^{III}Cl_9]^{3-}$ ion, 2.725(3) Å, with bond order one.[11e] The Ru–Ru distances are also notably longer than those of ruthenium blue complexes,[11d] $[Ru_2Cl_3(NH_3)_6]^{2+}$, 2.753(4) and $[Ru_2Cl_3(tacn)_2]^{2+}$, 2.830(1) Å. Thus, no Ru–Ru bond is predicted in $3^{+}I_3^{-}$. The Ru–Ru lengths compare well with those

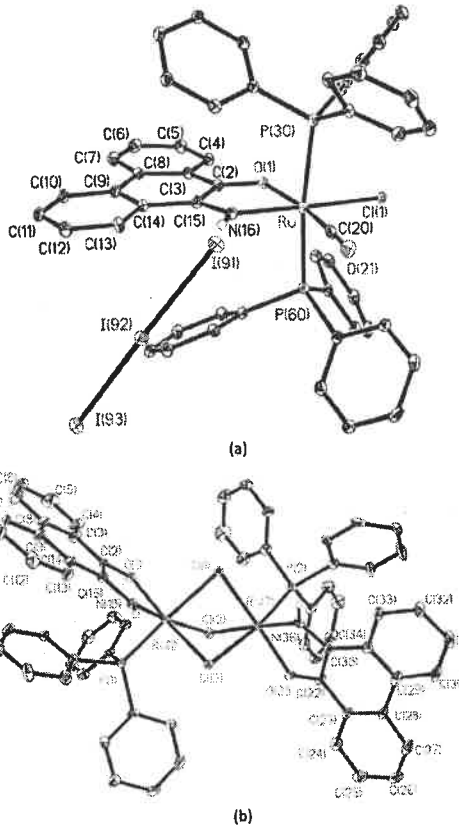

Fig. 4 Molecular geometries of (a) $1^{+}I_3^{-}\cdot\frac{1}{2}CH_2Cl_2$ (b) $3^{+}I_3^{-}\cdot\frac{1}{4}I_2\cdot\frac{1}{4}$toluene in crystals, with 40% thermal ellipsoids (I_3, I_2, CH_2Cl_2, toluene and H atoms are omitted for clarity as applicable).

complexes containing $[Ru^{III}(\mu\text{-}Cl)_3Ru^{III}]$ and $[Ru^{II}(\mu\text{-}Cl)_3Ru^{II}]$ cores.[11a,b] Expectedly, the average Ru–Cl–Ru angles of $3^{+}I_3^{-}\cdot\frac{1}{4}I_2\cdot\frac{1}{4}$toluene are relatively larger than those of ruthenium blue complexes.

The average Ru–O and Ru–N lengths, 2.057(8) and 1.947(9) Å, are similar to those of **2** and the average Ru–O/N lengths, 2.002(8) Å, are shorter than those of $1\cdot CH_2Cl_2$. The average C–O and C–N lengths, 1.273(14) and 1.304(14) Å, are relatively

Table 3 Selected experimental bond lengths (Å) and angles (°) of the four independent molecules present in the unit cell of $3^+I_3^-\cdot\frac{1}{4}I_2\cdot\frac{1}{4}$toluene

Bonds/angles	Molecule 1	Molecule 2	Molecule 3	Molecule 4
Ru–Ru	3.1582(12)	3.1470(12)	3.175(12)	3.183 (12)
Ru–N	1.954(9)/ 1.952(9)	1.948(9)/ 1.937(9)	1.953(9)/ 1.949(9)	1.932(9)/ 1.954(9)
Ru–O	2.047(8)/ 2.066(8)	2.053(7)/ 2.059(7)	2.058(7)/ 2.045(7)	2.084(8)/ 2.048(8)
Ru–P	2.297(3)/ 2.297(3)	2.293(3)/ 2.297(3)	2.311(3)/ 2.305(3)	2.301(3)/ 2.292(3)
Ru–Cl	2.407(3)/ 2.454(3)/ 2.482(3)/ 2.379(3)/ 2.428(3)/ 2.478(3)	2.392(3)/ 2.436(3)/ 2.487(3)/ 2.399(3)/ 2.438(3)/ 2.490(3)	2.414(3)/ 2.453(3)/ 2.472(3)/ 2.359(3)/ 2.445(3)/ 2.536(3)	2.372(3)/ 2.436(3)/ 2.518(3)/ 2.417(3)/ 2.435(3)/ 2.474(3)
C–O	1.277(14)/ 1.267(13)	1.264(14)/ 1.290(13)	1.264(13)/ 1.277(14)	1.273(14)/ 1.268(13)
C–N	1.299(15)/ 1.290(14)	1.301(14)/ 1.305(14)	1.315(14)/ 1.301(14)	1.319(14)/ 1.304(15)
C–C	1.474(17)/ 1.460(16)	1.433(16)/ 1.434(16)	1.443(15)/ 1.460(16)	1.442(16)/ 1.452(17)
Ru–Cl–Ru	81.00(8)/ 80.61(8)/ 80.54(8)	80.17(8)/ 80.25(8)/ 80.43(8)	82.14(8)/ 79.75(8)/ 80.81(8)	80.31(9)/ 82.10(9)/ 81.61(8)

longer than those of $4\cdot\frac{1}{2}CH_2Cl_2$. The average C–O/N, 1.288(14) and C–C lengths, 1.450(16) Å are similar to those observed in the cases of $PIQ^{\bullet-}$ in $1\cdot CH_2Cl_2$, $1^+I_3^-\cdot\frac{1}{2}CH_2Cl_2$ and **2**. Although the standard deviations of these lengths are higher, the trend infers that the 3^+ ion incorporates a bi-octahedral $[(PIQ^{\bullet-})Ru^{III}(\mu\text{-}Cl)_3Ru^{III}(PIQ^{\bullet-})]^+$ core. The average Ru–Cl lengths of the 3^+ ion are relatively shorter than those in $[Ru^{II}(\mu\text{-}Cl)_3Ru^{II}]$ cores but the lengths correlate well with those in the $[Ru^{III}(\mu\text{-}Cl)_3Ru^{III}]$ core.[11c] The average Ru–PPh_3 lengths of the 3^+ ion are similar to the Ru^{III}–PPh_3 lengths of $4\cdot\frac{1}{2}CH_2Cl_2$.

The 3^{2+} ion is paramagnetic and the frozen glass EPR spectrum at 115 K (Fig. S1(c)†) is anisotropic with g_1 = 2.485, g_2 = 2.010 and g_3 = 1.811 and the 3^{2+} ion is defined by the $[Ru_2^{III}(PIQ^{\bullet-})(PIQ)(PPh_3)_2(\mu\text{-}Cl)_3]^{2+}$ state. It is noteworthy that no EPR signal of the product obtained after coulometric reduction of $3^+I_3^-$ was detected predicting the instability of the neutral bi-octahedral core.

$5^+Br_3^-$ crystallizes in the *P2/n* space group. The molecular geometry with the atomic labelling scheme is shown in Fig. 5 and the selected bond parameters are listed in Table 4. The average Ru–O, Ru–P and Ru–Cl lengths are similar to those of *trans*-$[Ru^{II}(PQ)(PPh_3)_2(CO)Cl]^+$. The average C–O lengths, 1.253 (3) Å, are relatively shorter, while the C–C length (1.489(5) Å) of the chelate is longer correlating the existence of a quinoid ligand in the 5^+ ion, which is defined as a PQ complex of the ruthenium(III) ion.

Electrochemical studies

The redox activities of the complexes in CH_2Cl_2 were investigated by cyclic voltammetry at 295 K. The redox potential data referenced to the ferrocenium/ferrocene, Fc^+/Fc, couple are summarized in Table 5. The cyclic voltammograms of **1** and **2** are shown in Fig. 6 and others are depicted in Fig. S2.† The

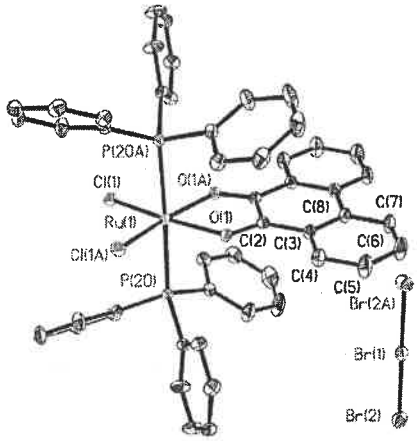

Fig. 5 Molecular geometry of $5^+Br_3^-$ in crystals, with 40% thermal ellipsoids (H atoms are omitted for clarity as applicable).

Table 4 Selected bond lengths (Å) of $5^+Br_3^-$

Ru(1)–O (avg)	2.063(2)
Ru(1)–Cl (avg)	2.289(2)
Ru(1)–P (avg)	2.418(2)
C(2)–O(1) (avg)	1.253(3)
C(2)–C(2A)	1.489(5)

Table 5 Redox potential data referenced to Fc^+/Fc couples determined by cyclic voltammetry in CH_2Cl_2 (0.20 M $[N(n\text{-}Bu)_4]PF_6$) at 295 K

Complexes	$E_{1/2}^{Ox1}$ (V) (ΔE^a, mV)	$E_{1/2}^{Ox2}$ (V) (ΔE^a, mV)	$E_{1/2}^{Red1}$ (V) (ΔE^a, mV)	$E_{1/2}^{Red2}$ (V) (ΔE^a, mV)
1	0.56 (91)	−0.45 (98)	−1.47[b]	
$1^+I_3^-$	0.20 (144)		−1.40 (138)	
2	0.20 (100)		−1.14 (102)	
$3^+I_3^-$	0.63 (100)	0.13 (153)	−0.76 (100)	−1.12 (148)
4			−0.02 (120)	−1.40[b]

[a] Peak to peak separation in mV. [b] Cathodic peak.

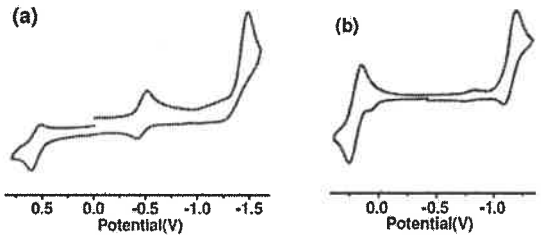

Fig. 6 Cyclic voltammograms of (a) **1** and (b) **2** in CH_2Cl_2 at 295 K. Conditions: scan rate, 100 in mV s^{-1}; 0.20 M $[N(n\text{-}Bu)_4]PF_6$ supporting electrolyte; platinum working electrode.

anodic wave of **1** at 0.56 V is assigned to the $Ru^{III}(PIQ^{\bullet-})/Ru^{II}(PIQ^{\bullet-})$ redox couple. The important observation is that the first cathodic wave of **1** at −0.45 V was initially absent, it was generated slowly during the scan in the range of +1.0 to −1.75

V as shown in Fig. S3.† It is proposed that during the measurements $Ru^{III}(PIQ^{\bullet-})$ slowly tautomerizes $Ru^{II}(PIQ)$ state which undergoes reduction at the cathode at −0.45 V as depicted in Fig. 6(a) and the wave is assigned to the $Ru^{II}(PIQ)/Ru^{II}(PIQ^{\bullet-})$ redox couple. The second cathodic peak at −1.47 V due to $Ru^{III}(PIQ^{\bullet-})/Ru^{III}(PIQ^{2-})$ is irreversible. In the case of **2** the anodic wave due to the $Ru^{III}(PIQ)/Ru^{III}(PIQ^{\bullet-})$ redox couple appears at 0.20 V. The cathodic wave of **2** at −1.14 V is assigned to the $Ru^{III}(PIQ^{\bullet-})/Ru^{II}(PIQ^{\bullet-})$ redox couple, as $\mathbf{2}^-$ in CH_2Cl_2 at 295 K exhibits an EPR signal at 1.998 due to the presence of the $Ru^{II}(PIQ^{\bullet-})$ state as a major component. The redox activity of $\mathbf{1}^+I_3^-$ is similar to that of **2**, exhibiting reversible anodic and cathodic waves at 0.20 and −1.40 V. The anodic waves of $\mathbf{3}^+I_3^-$ at 0.63 and 0.13 V are assigned to $Ru^{III}(PIQ)/Ru^{III}(PIQ^{\bullet-})$ redox couples, while the cathodic waves due to $Ru^{III}(PIQ^{\bullet-})/Ru^{II}(PIQ^{\bullet-})$ reduction couples are at −0.76 and −1.12 V. No anodic wave of **4** was discernible, it displays a reversible cathodic wave at −0.02 V and an irreversible peak at −1.40 V due to $Ru^{III}(PIQ)/Ru^{III}(PIQ^{\bullet-})$ and $Ru^{III}(PIQ^{\bullet-})/Ru^{II}(PIQ^{\bullet-})$ redox couples. The study infers that the PIQ^{2-} state is not stable in these coordination spheres.

Electronic spectra

UV-vis/NIR absorption spectra of the complexes in CH_2Cl_2 are shown in Fig. 7. The absorption parameters are summarized in Table 6. The λ_{exp} of **1** at 560 nm is assigned to the $d_{Ru} \rightarrow \pi_{ISQ}$ transition, λ_{cal} of which is 582.23 nm obtained from the TD-DFT calculation on $\mathbf{1}^{Me}$ in CH_2Cl_2 using the CPCM model. The corresponding MLCT transition of **4** with the $[Ru^{III}(PIQ)]$ state is red shifted to 610 nm as given in Fig. 7(a), with a shoulder at 730 nm due to the t_{2g}^5 state of the ruthenium(III) ion as an acceptor. The corresponding λ_{cal} values for $\mathbf{4}^{Me}$ are 795.27, 740.00 and 600.25 nm. The λ_{max} of **1** at 560 nm is red shifted to 625 nm in $\mathbf{1}^+I_3^-$, the corresponding calculated wavelength is 588.81 nm. **2** displays a sharper absorption band at 585 nm as depicted in Fig. 7(b), the calculated wavelength of $\mathbf{2}^{Me}$ for $d_{Ru} \rightarrow d_{Ru} + \pi_{ISQ}$ transitions is 529.07 nm. Similar to **2**, $\mathbf{3}^+I_3^-$ presents a similar transition at 672 nm and both are defined by $[Ru^{III}(PIQ^{\bullet-})]$ states. The UV-vis absorption spectrum of the $\mathbf{5}^+$ ion is similar to that of **4** as shown in Fig. S4.†

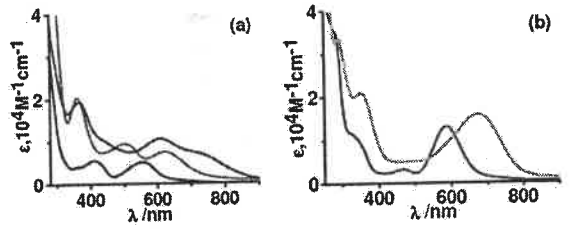

Fig. 7 UV-vis/NIR spectrum of (a) **1** (black), $\mathbf{1}^+I_3^-\cdot\frac{1}{2}CH_2Cl_2$ (red) and $\mathbf{4}\cdot\frac{1}{2}CH_2Cl_2$ (blue) (b) **2** (violet), and $\mathbf{3}^+I_3^-\cdot\frac{1}{4}I_2\cdot\frac{1}{4}$toluene (green) in CH_2Cl_2 at 295 K.

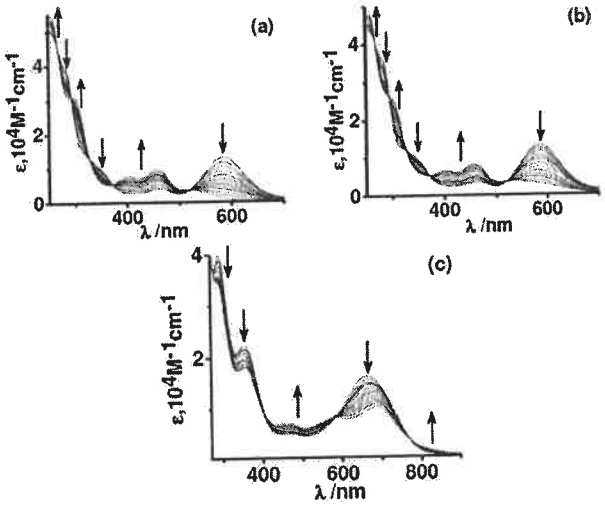

Fig. 8 Spectroelectrochemical measurements showing the change in electronic spectra during the conversions of (a) $\mathbf{2} \rightarrow \mathbf{2}^+$, (b) $\mathbf{2} \rightarrow \mathbf{2}^-$ and (c) $\mathbf{3}^+ \rightarrow \mathbf{3}^{2+}$ CH_2Cl_2 at 295 K.

The electronic spectra of $\mathbf{2}^+$, $\mathbf{2}^-$ and $\mathbf{3}^{2+}$ ions were recorded by spectroelectrochemical measurements in CH_2Cl_2 and the spectra are illustrated in Fig. 8. The change in the absorption feature during the conversions of $\mathbf{2} \rightarrow \mathbf{2}^+$ and $\mathbf{2} \rightarrow \mathbf{2}^-$ is notably similar, the intensity of the λ_{max} of **2** at 585 nm in both cases gradually diminishes. It is analyzed that the features of the electronic spectrum of the $\mathbf{2}^-$ ion are similar to those of **1** with the $[Ru^{II}(PIQ^{\bullet-})]$ state. Electronic spectra of the $\mathbf{3}^{2+}$ ion are illustrated in Fig. 8(c). The λ_{max} of the $\mathbf{3}^+$ ion at 671 nm is red shifted to 692 nm for the $\mathbf{3}^{2+}$ ion.

Table 6 Electronic spectra of **1**, $\mathbf{1}^+I_3^-\cdot\frac{1}{2}CH_2Cl_2$, **2**, $\mathbf{2}^+$, $\mathbf{2}^-$, $\mathbf{3}^+I_3^-\cdot\frac{1}{4}I_2\cdot\frac{1}{4}$toluene, $\mathbf{3}^{2+}$ and $\mathbf{4}\cdot\frac{1}{2}CH_2Cl_2$ in CH_2Cl_2 at 295 K

Complexes	λ_{max} (nm) (ε, 10^4 M^{-1} cm^{-1})
1	560 (0.52), 410 (0.55), 361 (0.4), 264 (4.45)
$\mathbf{1}^+I_3^-$	625 (0.75), 500 (0.95), 360 (2.03), 287 (5.7)
2	585 (1.31), 465 (0.31), 330 (1.10), 284 (3.6)
$\mathbf{2}^+$	525 (0.36), 457 (0.97), 400 (0.76), 300(3.10)
$\mathbf{2}^-$	550 (0.37), 457 (0.81), 403 (0.65), 300 (2.56)
$\mathbf{3}^+I_3^-$	672 (1.60), 470 (0.51), 353 (2.10), 292 (3.36)
$\mathbf{3}^{2+}$	692 (1.02), 576 (0.83), 468 (0.72), 356 (1.79)
4	730 (0.71), 610 (1.07), 440 (1.04), 366 (1.94)
$\mathbf{5}^+Br_3^-$	700 (0.85), 630 (0.76), 545 (0.48), 385 (1.05)

Experimental

Materials and physical measurements

Reagents or analytical-grade materials were obtained from commercial suppliers and used without further purification. The precursors $[Ru^{II}(PPh_3)_3(CO)HCl]$ and $[Ru^{II}(PPh_3)_3Cl_2]$ were prepared by reported procedures.[7] Spectroscopic-grade solvents were used for spectroscopic and electrochemical measurements. The C, H, and N contents of the compounds were obtained from a PerkinElmer 2400 Series II elemental analyzer. The elemental analyses were performed after

evaporating the solvents under high vacuum. Infrared spectra of the samples were recorded from 4000 to 400 cm^{-1} with KBr pellets at 295 K on a PerkinElmer Spectrum RX 1 Fourier transform infrared (FT-IR) spectrophotometer. ^1H NMR spectra in $CDCl_3$ were recorded on a Bruker DPX 300 MHz spectrometer. Electrospray ionization (ESI) mass spectra were recorded on a Micromass Q-TOF mass spectrometer. Electronic absorption spectra of the solutions of the complexes were recorded on a PerkinElmer Lambda 750 spectrophotometer in the range of 3300–175 nm. The X-band EPR spectra were recorded on a Magnettech GmbH MiniScope MS400 spectrometer (equipped with a temperature controller TC H03), where the microwave frequency was measured with an FC400 frequency counter. The EPR spectra were simulated using EasySpin software. The electro-analytical instrument, BASi Epsilon-EC for cyclic voltammetric experiments in CH_2Cl_2 containing 0.2 M tetrabutylammoniumhexafluorophosphate as a supporting electrolyte, was used. The BASi platinum working electrode, platinum auxiliary electrode, and Ag/AgCl reference electrode were used for the measurements. The redox potential data were referenced *versus* the ferrocenium/ferrocene, Fc^+/Fc, couple. A BASi SEC-C thin-layer quartz glass spectroelectrochemical cell kit (light path length of 1 mm) with a platinum gauze working electrode and a SEC-C platinum counter electrode were used for spectroelectrochemistry measurements. All of the physicochemical data were collected on the isolated $[Ru^{II}(PIQ^{\cdot-})(PPh_3)_2(CO)Cl]\cdot CH_2Cl_2$ ($\mathbf{1}\cdot CH_2Cl_2$), $[Ru^{III}(PIQ^{\cdot-})(PPh_3)_2Cl_2]$ (**2**), $[Ru^{III}(PIQ^{\cdot-})(PPh_3)_2(CO)Cl]^+I_3^-\cdot\frac{1}{2}CH_2Cl_2$ ($\mathbf{1}^+I_3^-\cdot\frac{1}{2}CH_2Cl_2$), $[Ru^{III}_2(PIQ^{\cdot-})_2(PPh_3)_2(\mu\text{-}Cl)_3]^+I_3^-\cdot\frac{1}{4}I_2\cdot\frac{1}{4}$toluene ($\mathbf{3}^+I_3^-\cdot\frac{1}{4}I_2\cdot\frac{1}{4}$toluene) and $[Ru^{III}(PIQ)(PPh_3)Br_3]\cdot\frac{1}{2}CH_2Cl_2$ ($\mathbf{4}\cdot\frac{1}{2}CH_2Cl_2$) complexes.

Syntheses

9,10-Phenanthreneiminoquinone (PIQ). PIQ was synthesized by a reported procedure.[6]

***trans*-$[Ru^{II}(PIQ^{\cdot-})(PPh_3)_2(CO)Cl]\cdot CH_2Cl_2$ (1).** To a solution of PIQ (20 mg, 0.1 mmol) in toluene (30 ml) $[Ru^{II}(PPh_3)_3(CO)(H)Cl]$ (100 mg, 0.1 mmol) was added and the mixture was refluxed for one hour under argon and allowed to cool at 295 K. A dark red crystalline product of $\mathbf{1}\cdot CH_2Cl_2$ separated out, it was filtered and dried in air. Yield: 65 mg (~72% with respect to ruthenium). Single crystals of $\mathbf{1}\cdot CH_2Cl_2$ for the X-ray diffraction study were grown by the diffusion of *n*-hexane into the CH_2Cl_2 solution of **1** at room temperature. Mass spectral data [electrospray ionization (ESI), positive ion, CH_2Cl_2]: *m/z* 896 for [**1**]. Anal. Calcd (%) for $C_{51}H_{39}ClNO_2P_2Ru$; C, 68.34; H, 4.39; N, 1.56. Found: C, 68.09; H, 4.38; N, 1.56. IR/cm^{-1} (KBr): ν 3388 (br, –NH), 3053 (m), 1928 (s, C≡O), 1601 (m), 1481 (s), 1434 (s), 1359 (s), 1096 (s), 731 (s), 693 (s), 519 (s).

***trans*-$[Ru^{III}(PIQ^{\cdot-})(PPh_3)_2Cl_2]$ (2).** To a solution of PIQ (20 mg, 0.1 mmol) in dry toluene (30 ml) $[Ru^{II}(PPh_3)_3Cl_2]$ (100 mg, 0.1 mmol) was added under argon and the solution was stirred at 353 K for 30 min. A dark solid of **2** separated out, which was filtered, and dried in air. Yield: 70 mg (~77% with respect to ruthenium). The slow diffusion of *n*-hexane into the CH_2Cl_2 solution of **2** in a glass tube at 295 K afforded single crystals of **2**, which were used for X-ray analyses, spectroscopic and electrochemical measurements. Mass spectral data [electrospray ionization (ESI) positive ion, CH_2Cl_2]: *m/z* 903 for [**2**]. Anal. Calcd (%) for $C_{50}H_{39}Cl_2NOP_2Ru$: C, 66.45; H, 4.35; N, 1.55. Found: C, 66.26; H, 4.33; N, 1.55. ^1H NMR ($CDCl_3$, 300 MHz): δ(ppm) 13.2 (1H, s), 8.81 (d, 2H), 8.07 (t, 2H), 7.93 (d, 2H), 7.81 (2H, d), 7.63–7.47 (15H, m), 7.36–7.26 (4H, m), 7.18–7.11 (11H, m). IR/cm^{-1} (KBr): ν 3402 (br, –NH), 3058 (m), 1599 (m), 1482 (s), 1433 (s), 1384 (s), 1319 (m), 1188 (m), 1093 (s), 745 (s), 693 (s), 511 (s).

***trans*-$[Ru^{III}(PIQ^{\cdot-})(PPh_3)_2(CO)Cl]^+I_3^-\cdot\frac{1}{2}CH_2Cl_2$ ($\mathbf{1}^+I_3^-\cdot\frac{1}{2}CH_2Cl_2$).** To a solution of **1** (50 mg, 0.05 mmol) in CH_2Cl_2 (5 ml), an iodine (20 mg, 0.075 mmol) solution of *n*-hexane (10 ml) was added and it was allowed to diffuse at 295 K. After a few days, crystals of the oxidized analogue of **1** were separated out as $\mathbf{1}^+I_3^-\cdot\frac{1}{2}CH_2Cl_2$. It was filtered and crystals were dried in air. Yield: 38 mg (~55% with respect to ruthenium). The product was used for single-crystal X-ray structure determination, spectroscopic and electrochemical measurements. Mass (ESI, positive ion, CH_2Cl_2): *m/z* 896 for $[\mathbf{1}]^+$. Anal. Calcd (%) for $C_{51}H_{39}ClI_3NO_2P_2Ru$: C, 47.97; H, 3.08; N, 1.10. Found: C, 47.78; H, 3.07; N, 1.10. ^1H NMR ($CDCl_3$, 300 MHz): δ(ppm) 12.60 (s, 1H), 8.35 (d, 1H), 8.07 (dd, 2H), 7.90 (dd, 2H), 7.74–7.54 (m, 12H), 7.31–7.19 (m, 21H). IR/cm^{-1} (KBr): ν 3432 (br, –NH), 3053 (w), 2017 (s, C≡O), 1599 (m), 1481 (m), 1433 (m), 1382 (m), 1318 (m), 1094 (s), 750 (m), 696 (s), 517 (s).

***trans*-$[Ru^{III}_2(PIQ^{\cdot-})_2(PPh_3)_2(\mu\text{-}Cl)_3]^+I_3^-\cdot\frac{1}{4}I_2\cdot\frac{1}{4}$toluene ($\mathbf{3}^+I_3^-\cdot\frac{1}{4}I_2\cdot\frac{1}{4}$toluene).** To a solution of **2** (50 mg, 0.05 mmol) in CH_2Cl_2 (10 ml), iodine (20 mg, 0.078 mmol) was added. The mixture was stirred for 10 min in air. To this solution, dry toluene (15 ml) was added slowly and allowed to diffuse at 295 K. After a few days needle like crystals of $\mathbf{3}^+I_3^-\cdot\frac{1}{4}I_2\cdot\frac{1}{4}$toluene separated out, which were collected upon filtration in air. This crop was used for single-crystal X-ray diffraction and other analytical, spectroscopic and electrochemical studies. Yield: 40 mg (~44% with respect to ruthenium). Mass spectral data [electrospray ionization (ESI), positive ion, CH_2Cl_2]: *m/z* 606 for $\frac{1}{2}[\mathbf{3}\text{-}Cl]^{2+}$. Anal. Calcd (%) for $C_{64}H_{48}Cl_3I_3N_2O_2P_2Ru_2$: C, 47.21; H, 2.97; N, 1.72, Found: C, 47.02; H, 2.96; N, 1.72. ^1H NMR ($CDCl_3$, 300 MHz): δ(ppm) 13.4 (2H, s), 8.30 (d, 4H), 8.12 (d, 4H), 7.99 (t, 8H), 7.73–7.57 (8H, m), 7.50–7.44 (5H, m), 7.38–7.32 (3H, m), 7.26–7.12 (10H, m), 6.96 (d, 2H), 6.74 (t, 2H). IR/cm^{-1} (KBr): ν 3435 (br, –NH), 3053 (w), 1635 (w), 1600 (m), 1493 (m), 1434 (m), 1381 (s), 1316 (m), 1093 (m), 766 (m), 692 (s), 525 (s), 512 (s).

***mer*-$[Ru^{III}(PIQ)(PPh_3)Br_3]\cdot\frac{1}{2}CH_2Cl_2$ ($\mathbf{4}\cdot\frac{1}{2}CH_2Cl_2$).** To a solution of **2** (50 mg, 0.05 mmol) in CH_2Cl_2 (10 ml), bromine (2 drops) was added. The mixture was stirred for 10 min in air. To this solution *n*-hexane (20 ml) was added slowly and allowed to diffuse at 295 K. After a few days green crystals of $\mathbf{4}\cdot\frac{1}{2}CH_2Cl_2$ were separated out, which were collected upon filtration in air. The crystals were used for single crystal X-ray diffraction and all other measurements. Yield: 15 mg (~37% with respect to ruthenium). Mass spectral data [electrospray ionization (ESI), positive ion, CH_2Cl_2]: *m/z* 734 for $[\mathbf{4}\text{-}Br]^+$. Anal. Calcd (%) for $C_{32}H_{24}Br_3NOPRu$: C, 47.43; H, 2.99; N, 1.73. Found: C, 47.26; H, 2.99; N, 1.73. IR/cm^{-1} (KBr): ν 3435 (br), 3053 (w), 1635 (m),

1621 (w), 1481 (m), 1450 (m), 1434 (s), 1386 (s), 1315 (m), 1093 (s), 761 (s), 694 (s), 520 (s).

trans-$[Ru^{III}(PQ)(PPh_3)_2Cl_2]^+Br_3^-$ ($5^+Br_3^-$). To a solution of $[Ru^{III}(PQ^{\bullet-})(PPh_3)_2Cl_2]$ (2_{PQ})[5] (50 mg, 0.05 mmol) in CH_2Cl_2 (5 ml), bromine (2 drops) was added. The mixture was stirred for 10 min under argon. To this solution *n*-hexane (20 ml) was added slowly and allowed to diffuse at 295 K. After a few days, crystals of $5^+Br_3^-$ were separated out, which were filtered and dried in air. Yield: 16 mg (~38% with respect to ruthenium). The product was used for single-crystal X-ray structure determination and spectroscopic measurement. Mass (ESI, positive ion, CH_2Cl_2): *m*/*z* 903 for $[5]^+$. Anal. Calcd (%) for $C_{50}H_{38}Cl_2Br_3O_2P_2Ru$: C, 52.47; H, 3.35. Found: C, 52.17; H, 3.34. IR/cm^{-1} (KBr): ν 3059 (m), 1647 (m), 1595 (s), 1482 (s), 1433 (s), 1361 (s), 1315 (m), 1094 (s), 741 (m), 690 (s), 516 (s).

Single-crystal X-ray structure determinations of the complexes (CCDC 1442782–1442786, 1454005)

Single crystals of $1{\cdot}CH_2Cl_2$, $1^+I_3^-{\cdot}\frac{1}{2}CH_2Cl_2$, **2**, $3^+I_3^-{\cdot}\frac{1}{4}I_2{\cdot}\frac{1}{4}$toluene, $4{\cdot}\frac{1}{2}CH_2Cl_2$ and $5^+Br_3^-$ were coated with perfluoropolyether picked up with nylon loops and mounted on Bruker APEX-II CCD and Bruker AXS D8 QUEST ECO diffractometers equipped with a Mo/Cu-target rotating-anode X-ray source and a graphite monochromator (Mo Kα, λ = 0.71073 Å). Radiation from a molybdenum X-ray source (Mo Kα, λ = 0.71073 Å) was used for all the complexes except for $1^+I_3^-{\cdot}\frac{1}{2}CH_2Cl_2$ which was measured with copper radiation (Cu Kα, λ = 1.54178 Å). Final cell constants were obtained from least squares fits of all measured reflections. Intensity data were corrected for absorption using intensities of redundant reflections. Structures were readily solved by direct methods and subsequent difference Fourier techniques. Details about software used for data collection, absorption correction, solution and refinement of the structures are given in the Crystallographic Information Files. The Siemens SHELXS-97 [12a] software package was used for solution, and SHELXL-97 [12b] was used for the refinement and XS. Ver. 2013/1,[12c] XT. Ver. 2014/4 [12d] and XL. Ver. 2014/7 [12e] were used for the structure solution and refinement. All non-hydrogen atoms were refined anisotropically. Hydrogen atoms were placed at the calculated positions and refined as riding atoms with isotropic displacement parameters. Crystallographic data of $1{\cdot}CH_2Cl_2$, $1^+I_3^-{\cdot}\frac{1}{2}CH_2Cl_2$, **2**, $3^+I_3^-{\cdot}\frac{1}{4}I_2{\cdot}\frac{1}{4}$toluene, $4{\cdot}\frac{1}{2}CH_2Cl_2$ and $5^+Br_3^-$ are listed in Table S1.†

The neutral complex $1{\cdot}CH_2Cl_2$ resides on a crystallographic two fold axis which therefore leads to disorder of the PIQ, CO and Cl^- ligands. Coordinates and displacement parameters of atoms N9 and O1 in PIQ were restrained to be equal using EXYZ and EADP instructions of SHELXL. Disordered Cl and CO atoms were refined without restraints due to the sufficient distance of density maxima and very low thermal displacement parameters. A disordered CH_2Cl_2 solvent molecule was located slightly off a crystallographic twofold axis. An occupation factor of 0.5 was used for the carbon and chlorine atoms and the C–Cl distances were refined to be equal within errors using the SADI instruction of SHELXL.

$1^+I_3^-{\cdot}\frac{1}{2}CH_2Cl_2$ crystallizes with 0.5 moles of CH_2Cl_2 residing on a crystallographic twofold axis. The solvent molecule was found to be disordered. The C–Cl (1.72 Å) and Cl–Cl (2.86 Å) distances were restrained to be equal using the SHELXL DFIX instruction.

The neutral complex **2** also crystallizes on a crystallographic twofold axis which leads to the same disorder problems as described for $1{\cdot}CH_2Cl_2$. Two voids of about 760 Å^3 (~29% of the total cell volume) containing a disordered solvent were detected after refinement of the complex molecule. Distribution of the density peaks suggested toluene to be present in the voids. Attempts to refine the toluene molecule showed that there is also some amount of dichloromethane present (solvent mixture from which crystals were grown). Unfortunately no satisfying disorder model could be refined and PLATON/Squeeze[12f,g] was used to remove scattering contributions from disordered solvents. A total of 146 electrons per void was calculated which roughly accounts for two toluene and one dichloromethane molecule per void.

The crystal structure of $3^+I_3^-{\cdot}\frac{1}{4}I_2{\cdot}\frac{1}{4}$toluene is clearly of a moderate quality. It crystallizes in the chiral space group $P2_1$ with four crystallographically independent cationic complex ions, four I_3^- anions, a neutral iodine molecule and a toluene as a solvent (Z = 8). The structure was refined as an inversion twin giving a scaling factor of about 0.44. A severely disordered I_2 unit resides between two almost co-parallel I_3^- anions (I1, I2, I3 and I31, I32, I33) bridging the two in an asymmetric fashion and forming a U-shaped I_8^{2-} dianionic unit. Much effort was made to model this disorder. The best result was achieved by a split atom model in which the I_2 (I34, I35) and one of the I_3^- subunits (I31, I32, I33) were split on two positions with an occupation ratio of about 0.83 : 0.17. EADP and SAME instructions of SHELXL were used to restrain the model. Residual density peaks (heaviest peak is 4.7 e Å^{-3} at a distance of 0.93 Å to I3) clearly show that the model does not fit the disorder perfectly but accounts for most of the problems. The refined structure model leaves small voids of a volume of about 104 Å^3 each. No significant electron density could be found in these voids.

An occupation factor of 0.5 was used for the carbon and chlorine atoms to refine the structure of $4{\cdot}\frac{1}{2}CH_2Cl_2$.

Density functional theory (DFT) calculations

All calculations reported in this article were done with the Gaussian 03W[13] program package supported by GaussView 4.1. The DFT[14] and time-dependent (TD) DFT[15] calculations were performed at the level of Becke three parameter hybrid functional with the nonlocal correlation functional of Lee–Yang–Parr (B3LYP).[16] The gas-phase geometries of *trans*-$[Ru^{II}(PIQ)(PMe_3)_2(CO)Cl]^+$ (1^{Me+}) and *trans*-$[Ru^{III}(PIQ^{\bullet-})(PMe_3)_2Cl_2]$ (2^{Me}) were optimized with the singlet spin state. The gas-phase geometries of *trans*-$[Ru^{II}(PIQ^{\bullet-})(PMe_3)_2(CO)Cl]$ (1^{Me}), *trans*-$[Ru^{III}(PIQ)(PMe_3)_2Cl_2]^+$ (2^{Me+}), *trans*-$[Ru^{II}(PIQ^{\bullet-})(PMe_3)_2Cl_2]^-$ (2^{Me-}) and *mer*-$[Ru^{III}(PIQ)(PMe_3)Br_3]$ (4^{Me}) were optimized with the doublet spin state, using Pulay's Direct Inversion[17] in the Iterative Subspace (DIIS), and the "tight"

convergent self consistent field procedure[18] ignoring the symmetry. In all calculations, a LANL2DZ basis set along with the corresponding effective core potential (ECP) was used for the ruthenium ion.[19] The valence double-ζ basis set, 6-31G for H was used.[20] For C, N, P, Cl, and Br non-hydrogen atoms, valence double-ζ with diffuse and polarization functions, 6-31++G** as the basis set[21] were employed for all calculations. The 60 lowest singlet excitation energies on each of the optimized geometries of $\mathbf{1}^{Me}$, $\mathbf{2}^{Me+}$, $\mathbf{2}^{Me-}$ and $\mathbf{4}^{Me}$ were elucidated by TD DFT calculations. The nature of transitions was calculated by adding the probability of the same type among α and β molecular orbitals.

Conclusions

The redox non-innocence of 9,10-phenanthreneimino quinone (PIQ), the coordination chemistry of which was limited, reveals the diverse electronic states with ruthenium(II/III) ions as depicted in Scheme 2. The electronic states of the [Ru(PIQ)] core of types $[Ru^{II}(PIQ^{\bullet-})]$, $[Ru^{III}(PIQ^{\bullet-})]$, $[Ru_2^{III}(PIQ^{\bullet-})_2]$, $[Ru_2^{III}(PIQ^{\bullet-})(PIQ)]$ and $[Ru^{III}(PIQ)]$ were detected ($PIQ^{\bullet-}$ = 9,10-phenanthreneiminoquinonate anion radical) and compared with those of 9,10-phenanthrenequinone (PQ) complexes of ruthenium(II/III) ions.

In this article, the molecular and electronic structures of *trans*-$[Ru^{II}(PIQ^{\bullet-})(PPh_3)_2(CO)Cl]\cdot CH_2Cl_2$ ($\mathbf{1}\cdot CH_2Cl_2$), *trans*-$[Ru^{III}(PIQ^{\bullet-})(PPh_3)_2Cl_2]$ (**2**), *trans*-$[Ru^{III}(PIQ^{\bullet-})(PPh_3)_2(CO)Cl]^+I_3^-\cdot\frac{1}{2}CH_2Cl_2$ ($\mathbf{1}^+I_3^-\cdot\frac{1}{2}CH_2Cl_2$), *trans*-$[Ru_2^{III}(PIQ^{\bullet-})_2(PPh_3)_2(\mu\text{-}Cl)_3]^+I_3^-\cdot\frac{1}{4}I_2\cdot\frac{1}{4}$toluene ($\mathbf{3}^+I_3^-\cdot\frac{1}{4}I_2\cdot\frac{1}{4}$toluene), *mer*-$[Ru^{III}(PIQ)(PPh_3)Br_3]\cdot\frac{1}{2}CH_2Cl_2$ ($\mathbf{4}\cdot\frac{1}{2}CH_2Cl_2$) and *trans*-$[Ru^{III}(PQ)(PPh_3)_2Cl_2]^+Br_3^-$ ($\mathbf{5}^+Br_3^-$) are reported. The single crystal X-ray bond parameters, EPR spectrum and density functional theory calculations predicted that **1** is a $PIQ^{\bullet-}$ complex of ruthenium(II), while **4** is a PIQ complex of ruthenium(III). $\mathbf{1}^+I_3^-\cdot\frac{1}{2}CH_2Cl_2$ and **2** are defined as $PIQ^{\bullet-}$ complexes of ruthenium(III). Based on the single crystal X-ray bond parameters of the chelate and UV-vis/NIR absorption spectra, $\mathbf{3}^+I_3^-\cdot\frac{1}{4}I_2\cdot\frac{1}{4}$toluene is defined as a co-facial bi-octahedral ruthenium complex that contains the $[(PIQ^{\bullet-})\text{-}Ru^{III}(\mu\text{-}Cl)_3Ru^{III}(PIQ^{\bullet-})]^+$ core. However, the PQ analogue of **2**, *trans*-$[Ru^{III}(PQ^{\bullet-})\text{-}(PPh_3)_2Cl_2]$ ($\mathbf{2}_{PQ}$), reacts differently with Br_2 affording *trans*-$[Ru^{III}(PQ)(PPh_3)_2Cl_2]^+Br_3^-$ ($\mathbf{5}^+Br_3^-$) only, authenticated by a single crystal X-ray diffraction study. Considering the EPR spectra and the atomic spin densities, the 2^+ ion is described as a PIQ complex of ruthenium(III), while the 2^- ion is a hybrid state of the $[Ru^{II}(PIQ^{\bullet-})]$ and $[Ru^{III}(PIQ^{2-})]$ states. It can be inferred that in complexes PIQ acts as a one electron sink and in most cases exists as $PIQ^{\bullet-}$ in which a significant percentage of the atomic spin is localized on a nitrogen p-orbital (calculated, ~38% in **1** and ~35% in 2^- ion), while the PIQ^{2-} state with the ruthenium ion has so far not been detected.

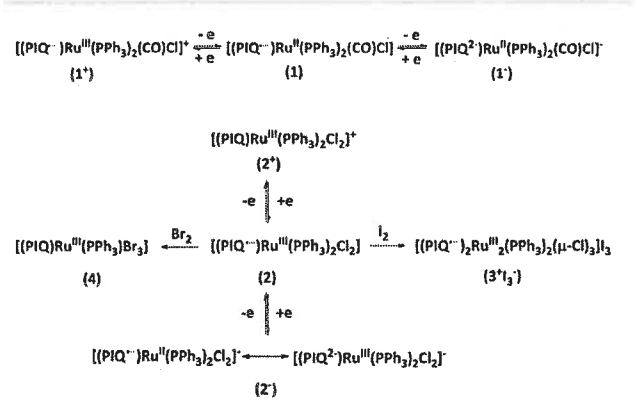

Scheme 2 Diverse electronic states of [Ru(PIQ)] core in complexes.

Acknowledgements

Financial support received from the Department of Science and Technology (SR/S1/IC/0026/2012) and Council of Scientific and Industrial Research 01(2699/12/EMR-II), New Delhi, India is gratefully acknowledged. S. B. (08/531(0006)/2012-EMR-I) and S. M. (08/531(0004)/2010-EMR-I) are thankful to CSIR, New Delhi, India, for fellowships.

References

1 (*a*) D. L. J. Broere, R. Plessius and J. I. Vlugt, *Chem. Soc. Rev.*, 2015, **44**, 6886–6915; (*b*) M. E. O'Reilly and A. S. Veige, *Chem. Soc. Rev.*, 2014, **43**, 6325–6369; (*c*) O. R. Luca and R. H. Crabtree, *Chem. Soc. Rev.*, 2013, **42**, 1440–1459.

2 (*a*) G. Skara, B. Pinter, P. Geerlings and F. De Proft, *Chem. Sci.*, 2015, **6**, 4109–4117; (*b*) M. Wang, J. England, T. Weyhermüller and K. Wieghardt, *Inorg. Chem.*, 2014, **53**, 2276–2287; (*c*) S. C. Patra, A. Saha Roy, V. Manivannan, T. Weyhermüller and P. Ghosh, *Dalton Trans.*, 2014, **43**, 13731; (*d*) A. Kochem, G. Gellon, O. Jarjayes, C. Philouze, N. Leconte, M. Gastel, E. Bill and F. Thomas, *Chem. Commun.*, 2014, **50**, 4924–4926; (*e*) H. Agarwala, T. M. Scherer, S. M. Mobin, W. Kaim and G. K. Lahiri, *Dalton Trans.*, 2014, **43**, 3939–3948; (*f*) A. I. O. Suarez, V. Lyaskovskyy, J. N. H. Reek, J. I. Vlugt and B. de Bruin, *Angew. Chem., Int. Ed.*, 2013, **52**, 12510–12529; (*g*) M. K. Biswas, S. C. Patra, A. N. Maity, S.-C. Ke, N. Das Adhikary and P. Ghosh, *Inorg. Chem.*, 2012, **51**, 6687–6699; (*h*) A. B. P. Lever, *Coord. Chem. Rev.*, 2010, **254**, 1397–1405; (*i*) W. Kaim and B. Schwederski, *Coord. Chem. Rev.*, 2010, **254**, 1580–1588; (*j*) A. I. Poddel'sky, V. K. Cherkasov and G. A. Abakumov, *Coord. Chem. Rev.*, 2009, **253**, 291–324; (*k*) R. A. Zarkesh, J. W. Ziller and A. F. Heyduk, *Angew. Chem., Int. Ed.*, 2008, **47**, 4715–4718; (*l*) C. Remenyi and M. Kaupp, *J. Am. Chem. Soc.*, 2005, **127**, 11399–11413; (*m*) E. Bill, E. Bothe, P. Chaudhuri, K. Chlopek, D. Herebian, S. Kokatam, K. Ray, T. Weyhermüller, F. Neese and K. Wieghardt, *Chem. – Eur. J.*, 2005, **11**, 204–224; (*n*) C. G. Pierpont, *Coord. Chem. Rev.*, 2001, **219–221**, 415–433.

3 (*a*) A. Kochem, G. Gellon, O. Jarjayes, C. Philouze, A. M. d'Hardemare, M. Gastel and F. Thomas, *Dalton Trans.*, 2015, **44**, 12743–12756; (*b*) A. V. Piskunov, I. N. Meshcheryakova, I. V. Ershova, A. S. Bogomyakov, A. V. Cherkasov and G. K. Fukin, *RSC Adv.*, 2014, **4**, 42494–42505; (*c*) A. Rajput, A. K. Sharma, S. K. Barman, D. Koley, M. Steinert and R. Mukherjee, *Inorg. Chem.*, 2014, **53**, 36–48; (*d*) R. Rakshit, S. Ghorai, S. Biswas and C. Mukherjee, *Inorg. Chem.*, 2014, **53**, 3333–3337; (*e*) S. Hananouchi, B. T. Krull, J. W. Ziller, F. Furche and A. F. Heyduk, *Dalton Trans.*, 2014, **43**, 17991–18000; (*f*) S. Kundu, S. Maity, A. N. Maity, S.-C. Ke and P. Ghosh, *Dalton Trans.*, 2013, **42**, 4586–4601; (*g*) A. Saha Roy, P. Saha, N. Das Adhikary and P. Ghosh, *Inorg. Chem.*, 2011, **50**, 2488–2500; (*h*) S. Mukherjee, T. Weyhermüller, K. Wieghardt and P. Chaudhuri, *Dalton Trans.*, 2003, 3483–3485.

4 (*a*) A. Mandal, T. Kundu, F. Ehret, M. Bubrin, S. M. Mobin, W. Kaim and G. K. Lahiri, *Dalton Trans.*, 2014, **43**, 2473; (*b*) E. Balogh-Hergovich and G. Speier, *Inorg. Chim. Acta*, 1984, **84**, 129–134.

5 (*a*) M. K. Biswas, S. C. Patra, A. N. Maity, S.-C. Ke, T. Weyhermüller and P. Ghosh, *Dalton Trans.*, 2013, **42**, 6538–6552; (*b*) M. K. Biswas, S. C. Patra, A. N. Maity, S.-C. Ke, N. Das Adhikary and P. Ghosh, *Inorg. Chem.*, 2012, **51**, 6687–6699; (*c*) S. Bhattacharya, P. Gupta and F. Basuli, *Inorg. Chem.*, 2002, **41**, 5810–5816; (*d*) M. Shivakumar, K. Pramanik, P. Ghosh and A. Chakravorty, *Inorg. Chem.*, 1998, **37**, 5968.

6 (*a*) J. Schmidt and E. Junghans, *Chem. Ber.*, 1904, **37**, 3558; (*b*) R. Pschorr, *Chem. Ber.*, 1902, **35**, 2739.

7 (*a*) N. Ahmad, J. J. Levison, S. D. Robinson and M. F. Uttley, *Inorg. Synth.*, 1974, **15**, 45; (*b*) T. A. Stephenson and G. J. Wilkinson, *Inorg. Nucl. Chem.*, 1966, **28**, 945.

8 (*a*) L. Dubicki and E. Krausz, *Inorg. Chem.*, 1985, **24**, 4461; (*b*) N. S. Hush, J. K. Beattie and V. M. Ellis, *Inorg. Chem.*, 1984, **23**, 3339.

9 (*a*) S.-L. Kokatam, P. Chaudhuri, T. Weyhermüller and K. Wieghardt, *Dalton Trans.*, 2007, 373–378; (*b*) K. S. Min, T. Weyhermüller and K. Wieghardt, *Dalton Trans.*, 2003, 1126–1132.

10 (*a*) A. V. Piskunov, I. V. Ershova, A. S. Bogomyakov, A. G. Starikov, G. K. Fukin and V. K. Cherkasov, *Inorg. Chem.*, 2015, **54**, 6090–6099; (*b*) M. K. Mondal, A. K. Biswas, B. Ganguly and C. Mukherjee, *Dalton Trans.*, 2015, **44**, 9375–9381; (*c*) D. L. J. Broere, S. Demeshko, B. de Bruin, E. A. Pidko, J. N. H. Reek, M. A. Siegler, M. Lutz and J. I. Vlugt, *Chem. – Eur. J.*, 2015, **21**, 1–9; (*d*) M. Bubrin, D. Schweinfurth, F. Ehret, S. Záliš, H. Kvapilová, J. Fiedler, Q. Zeng, F. Hartl and W. Kaim, *Organometallics*, 2014, **33**, 4973–4985; (*e*) M. M. Bittner, D. Kraus, S. V. Lindeman, C. V. Popescu and A. T. Fiedler, *Chem. – Eur. J.*, 2013, **19**, 9686–9698; (*f*) S. E. Balaghi, E. Safaei, L. Chiang, E. W. Y. Wong, D. Savard, R. M. Clarke and T. Storr, *Dalton Trans.*, 2013, **42**, 6829; (*g*) S. Fuse, H. Tago, M. M. Maitani, Y. Y. Wada and T. Takahashi, *ACS Comb. Sci.*, 2012, **14**, 545–550; (*h*) P. Chaudhuri, C. N. Verani, E. Bill, E. Bothe, T. Weyhermüller and K. Wieghardt, *J. Am. Chem. Soc.*, 2001, **123**, 2213–2223.

11 (*a*) S. D. Drouin, S. Monfette, D. Amoroso, G. P. A. Yap and D. E. Fogg, *Organometallics*, 2005, **24**, 4721–4728; (*b*) D. Amoroso, G. P. A. Yap and D. E. Fogg, *Organometallics*, 2002, **21**, 3335–3343; (*c*) M. P. de Araujo, S. L. Queiroz, A. A. Batista, E. H. Panepucci, G. Oliva and E. E. Castellano, *Transition Met. Chem.*, 2002, **27**, 110–114; (*d*) W. A. Clucas, R. S. Armstrong, I. E. Buys, T. W. Hambley and K. W. Nugent, *Inorg. Chem.*, 1996, **35**, 6789–6794; (*e*) J. Darriet, *Rev. Chim. Miner.*, 1981, **18**, 27.

12 (*a*) G. M. Sheldrick, *ShelXS97*, Universität Göttingen, Göttingen, Germany, 1997; (*b*) G. M. Sheldrick, *ShelXL97*, Universität Göttingen, Göttingen, Germany, 1997; (*c*) G. M. Sheldrick, *XS. Version 2013/1*, Georg-August-Universität Göttingen, Göttingen, Germany, 2013; (*d*) G. M. Sheldrick, *Acta Crystallogr., Sect. A: Fundam. Crystallogr.*, 2015, **71**, 3–8; (*e*) G. M. Sheldrick, *Acta Crystallogr., Sect. C: Cryst. Struct. Commun.*, 2015, **71**, 3–8; (*f*) A. L. Spek, *Acta Crystallogr., Sect. D: Biol. Crystallogr.*, 2009, **65**, 148–155; (*g*) A. L. Spek, *Platon – A Multipurpose Crystallographic Tool*, Utrecht University, Utrecht, The Netherlands, 2011.

13 M. J. Frisch, G. W. Trucks, H. B. Schlegel, G. E. Scuseria, M. A. Robb, J. R. Cheeseman Jr., J. A. Montgomery, T. Vreven, K. N. Kudin, J. C. Burant, J. M. Millam, S. S. Iyengar, J. Tomasi, V. Barone, B. Mennucci, M. Cossi, G. Scalmani, N. Rega, G. A. Petersson, H. Nakatsuji, M. Hada, M. Ehara, K. Toyota, R. Fukuda, J. Hasegawa, M. Ishida, T. Nakajima, Y. Honda, O. Kitao, H. Nakai, M. Klene, X. Li, J. E. Knox, H. P. Hratchian, J. B. Cross, V. Bakken, C. Adamo, J. Jaramillo, R. Gomperts, R. E. Stratmann, O. Yazyev, J. A. Austin, R. Cammi, C. Pomelli, J. W. Ochterski, P. Y. Ayala, K. Morokuma, G. A. Voth, P. Salvador, J. J. Dannenberg, V. G. Zakrzewski, S. Dapprich, A. D. Daniels, M. C. Strain, O. Farkas, D. K. Malick, A. D. Rabuck, K. Raghavachari, J. B. Foresman, J. V. Ortiz, Q. Cui, A. G. Baboul, S. Clifford, J. Cioslowski, B. B. Stefanov, G. Liu, A. Liashenko, P. Piskorz, I. Komaromi, R. L. Martin, D. J. Fox, T. Keith, M. A. Al-Laham, C. Y. Peng, A. Nanayakkara, M. Challacombe, P. M. W. Gill, B. Johnson, W. Chen, M. W. Wong, C. Gonzalez and J. A. Pople, *GAUSSIAN 03 (Revision E.01)*, Gaussian, Inc., Wallingford, CT, 2004.

14 (*a*) R. G. Parr and W. Yang, *Density Functional Theory of Atoms and Molecules*, Oxford University Press, Oxford, UK, 1989; (*b*) D. R. Salahub and M. C. Zerner, *The Challenge of d and f Electrons, ACS Symposium Series 394*, American Chemical Society, Washington, DC, 1989; (*c*) W. Kohn and L. J. Sham, *Phys. Rev.*, 1965, **140**, A1133–A1138; (*d*) P. Hohenberg and W. Kohn, *Phys. Rev.*, 1964, **136**, B864–B871.

15 (*a*) R. E. Stratmann, G. E. Scuseria and M. Frisch, *J. Chem. Phys.*, 1998, **109**, 8218–8224; (*b*) M. E. Casida, C. Jamoroski, K. C. Casida and D. R. Salahub, *J. Chem. Phys.*, 1998, **108**, 4439–4449; (*c*) R. Bauernschmitt, M. Haser, O. Treutler and R. Ahlrichs, *Chem. Phys. Lett.*, 1996, **256**, 454–464.

16 (*a*) A. D. Becke, *J. Chem. Phys.*, 1993, **98**, 5648–5652; (*b*) B. Miehlich, A. Savin, H. Stoll and H. Preuss, *Chem.*

Phys. Lett., 1989, **157**, 200–205; (*c*) C. Lee, W. Yang and R. G. Parr, *Phys. Rev. B: Condens. Matter*, 1988, **37**, 785–789.
17 P. J. Pulay, *Comput. Chem.*, 1982, **3**, 556.
18 H. B. Schlegel and J. J. McDouall, in *Computational Advances in Organic Chemistry*, ed. C. Ogretir and I. G. Csizmadia, Kluwer Academic, The Netherlands, 1991, pp. 167–185.
19 (*a*) P. J. Hay and W. R. Wadt, *J. Chem. Phys.*, 1985, **82**, 270–283; (*b*) W. R. Wadt and P. J. Hay, *J. Chem. Phys.*, 1985, **82**, 284–298; (*c*) P. J. Hayand and W. R. Wadt, *J. Chem. Phys.*, 1985, **82**, 299–310.
20 (*a*) V. A. Rassolov, M. A. Ratner, J. A. Pople, P. C. Redfern and L. A. Curtiss, *J. Comput. Chem.*, 2001, **22**, 976–984; (*b*) M. M. Francl, W. J. Pietro, W. J. Hehre, J. S. Binkley, D. J. DeFrees, J. A. Pople and M. S. Gordon, *J. Chem. Phys.*, 1982, **77**, 3654–3665; (*c*) P. C. Hariharan and J. A. Pople, *Mol. Phys.*, 1974, **27**, 209–214; (*d*) P. C. Hariharan and J. A. Pople, *Theor. Chim. Acta*, 1973, **28**, 213–222; (*e*) W. J. Hehre, R. Ditchfield and J. A. Pople, *J. Chem. Phys.*, 1972, **56**, 2257–2261.
21 W. J. Hehre, R. Ditchfield and J. A. Pople, *J. Chem. Phys.*, 1972, **56**, 2257.